May, 2022

Cavity Quantum Electro-optic Effect

Undergraduate Honors Thesis

Rahaf Youssef [1]

Advisors:

Silvia Zorzetti[2,3] and Changqing Wang [2,3]

[1] Saint Olaf College, MN 55057

[2] Superconducting Quantum Materials and Systems Center, Batavia, IL 60510

[3] Fermi National Accelerator Laboratory, Batavia, IL 60510

Contents

1 Introduction

Quantum computing has garnered considerable attention in recent years due to its potential to break encryption (5), advance scientific computing (6), and perform molecular simulation (7), among many other applications. Recent advancements in the field allowed for developing multiple quantum computing platforms with high-fidelity one or two-qubit gates (8). As of now, there are various ways to realize a qubit: superconducting qubits (8), rare-earth solid-state qubits (9), photonic qubits (10), etc. While each platform offers a unique advantage, superconducting qubits are arguably the most advanced and well researched, demonstrating a high average thermal relaxation time of $\bar{T}_1 = 49\mu$s and dephasing time of $\bar{T}_2 = 95\mu$s (10). While low-noise superconducting qubits and the nonlinearity from the Josephson effect are crucial in developing quantum processors, optical photons are a natural choice for quantum networks due to their low-propagation noise in room-temperature environments (12). It is therefore crucial to develop coherent microwave-to-optical transducers to connect superconducting qubits and high-Q cavities with the aim of long-distance quantum information transfer (4).

There are multiple technologies to achieve the goal of quantum transduction. Most notably, there are electro-optic, electro-mechanical as well as atomic-based ensemble approaches (i.e. trapped neutral atoms and rare-earth-ion-doped crystals (3)). The focus of this project is on the former: utilizing the electro-optic effect in quantum transduction. Specifically, we are considering a microwave-optical superconducting transduction cavity with long coherence time (13). The cavity's 3D architecture allows for a high quality factor due to the smoothness and low resistance of the inner surface. When the cavity is cryogenically cooled to milli-Kelvin temperature, it has ultra-low resistivity, resulting

in a quality factor of Q = 10^{10} and hence, a photon lifetime of about 2 seconds (13; 14). We aim to utilize a full quantum treatment of the electro-optic effect to study the bidirectional microwave-optical conversion in different parameter regimes of the decay rates of the optical and microwave fields.

2   Quantum Transduction

Quantum transduction is the process of converting a quantum signal from one form of energy to another (3). This process has become an active area of research due to its potential to advance the fields of quantum science and technology. The promise of advancement emerges from the fact that transduction allows quantum information to be exchanged between remote quantum systems that operate at different energy scales. Since each quantum system has unique attributes that render it useful in performing specific tasks, a quantum transducer would allow us to exploit each quantum system to our advantage and connect these systems by exchanging signals between them. Consequently, just like bidirectional electrical and optical signal conversion is at the heart of global internet, quantum transducers can be the cornerstone of quantum internet, where remotely connected quantum systems can exchange information (4).

In this project, the focus is microwave-optical transduction, where the two modes are about five orders of magnitude apart. This means that the two modes have different frequencies, resulting in off-resonant interactions. In order for the two modes to interact, they need to be coherently coupled through an intermediary system. To that end, a full quantum treatment of the electro-optic coupling between the modes was developed by Matsko (1; 2). In this work, Matsko treats the optical and microwave fields as quantum degrees of freedom and studies their coupling through the electro-optic effect, where the

two fields are considered to be modes in a cavity or resonator (1). His work provides the main theoretical framework for this project.

3   Experimental Setup

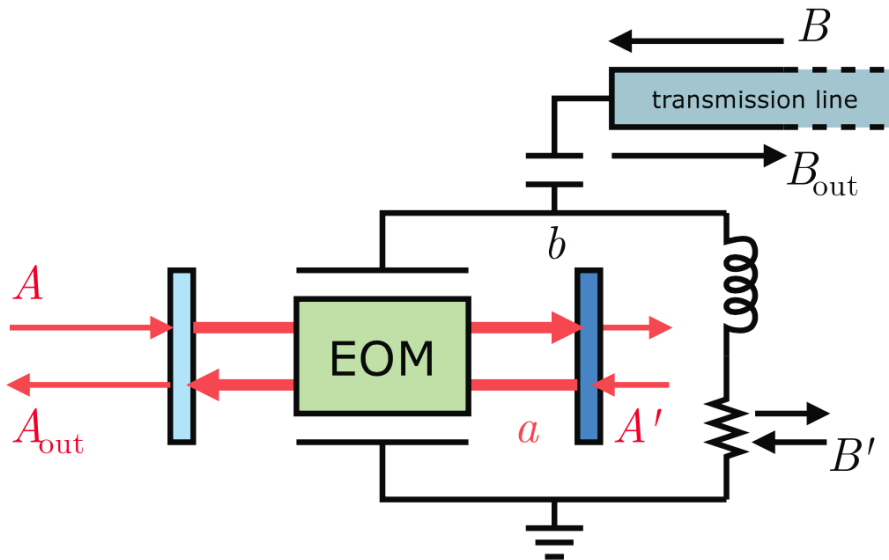To achieve the desired electro-optic conversion, the setup shown in Figure 1 is used.

Figure 1: Schematic of electro-optic Transducer (1)

.

In this setup, there is an LC circuit, where there is an inductor and a capacitor. The microwave signal is coming through the transmission line, which is indicated by the horizontal blue rectangle on the top right corner of Figure 1. The LC circuit and the transmission line combined make up the microwave resonator. Furthermore, there is an optical cavity whose mirrors are represented by the vertical blue rectangles. Inside this cavity, there is electro-optic modulator (EOM), which modulates the electrical signal to an optical one. Again, one of the goals of this project is a full quantum treatment of

the electro-optic effect, and hence the quantum creation and annihilation operators that are shown in Figure 1. More specifically, A & A_{out} are the input and output optical field annihilation operators, B & B_{out} are the input and output microwave field annihilation operators, and A' & B' are the quantum Langevin noise operators coupled through parasitic losses in the optical and microwave resonators, respectively.

As previously mentioned, the EOM modulates a given electrical signal into an optical one. Hence, building a converter that changes a given signal from an electrical to an optical one, we need a three-wave mixing process, which is shown in Figure 2. This non-linear medium is located inside the EOM.
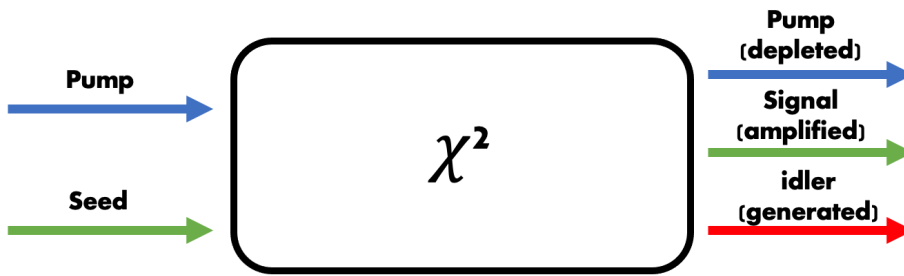

Figure 2: Diagram of the three-wave mixing process

As shown in Figure 2, there is a pump laser beam and an optical signal, and they are sent through a nonlinear crystal (such as Potassium Titanyl Phosphate or Lithium Niobate), where they both mix. This crystal exhibits electro-optic non-linearity, which means that, when high-intensity electric field is applied to it, the refractive index of this nonlinear crystal is modulated, i.e. the phase of the optical wave will be modulated too. As a result, the pump frequency is depleted, and an optical signal is produced and amplified along with a microwave signal. That way, we end up with the desired optical signal.

4   Theoretical Background

To develop the Hamiltonian representing this system, we can start by the following single-mode optical interaction Hamiltonian:

$$H_I = -\frac{\hbar}{\tau}\phi a^\dagger a, \tag{1}$$

where a and $a^\dagger$ optical annihilation and creation operators, τ is the optical round-trip time, and ϕ is the single-round-trip phase shift. Let $\phi = \frac{\omega_a n^3 rl}{cd}V$, where n is the optical refractive index inside the electro-optic medium, r is the electro-optic coefficient, l is the length of the medium along the optical axis, d is the thickness, and V is the voltage across the medium.

The interaction Hamiltonian then becomes

$$H_I = -\frac{\hbar}{\tau}\left(\frac{\omega_a n^3 rl}{cd}V\right)a^\dagger a \tag{2}$$

If the modulator is treated as a capacitor in a single-mode microwave resonator, voltage is quantized according to this relation: $V = \sqrt{\frac{\hbar\omega_b}{2C}}(b + b^\dagger)$, where b and $b^\dagger$ are the microwave annihilation and creation operators, respectively, ω_b is the microwave resonant frequency, and C is the capacitance of the microwave resonator.

Plug Equation 3 into Equation 2, so the interaction Hamiltonian becomes

$$H_I = -\frac{\hbar}{\tau}\left(\frac{\omega_a n^3 rl}{cd}\right)\left(\sqrt{\frac{\hbar\omega_b}{2C}}(b+b^\dagger)\right)a^\dagger a = -\hbar g(b+b^\dagger)a^\dagger a, \tag{3}$$

where $g = \frac{\omega_a n^3 rl}{c\tau d}\sqrt{\frac{\hbar\omega_b}{2C}}$.

The full Hamiltonian consists of the interaction Hamiltonian and two free terms for ω_a and ω_b as follows

$$H = \hbar\omega_a a^\dagger a + \hbar\omega_b b^\dagger b - \hbar g(b+b^\dagger)a^\dagger a \tag{4}$$

We can only consider three optical modes if $|\Delta\omega - \omega_b| \gg \gamma_a$, where γ_a is the optical linewidth. These three modes are represented by the center optical mode, red-detuned mode, and blue-detuned mode, as shown in Figure 3.
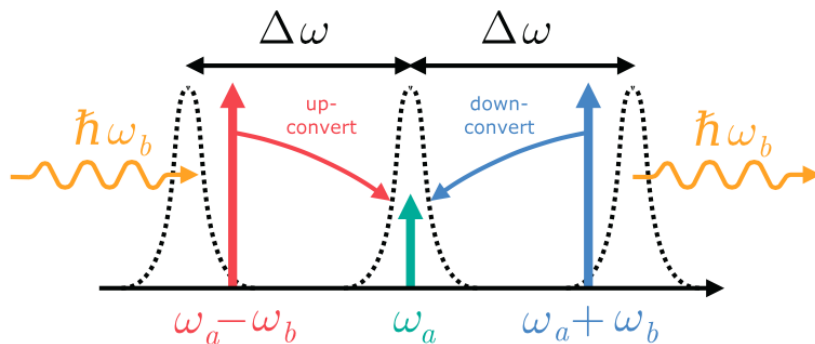

Figure 3: Red-detuned optical pumping cools the microwave mode by transferring energy from the microwave to the optical mode at ω_a via parametric up-conversion. Blue-detuned pumping causes nondegenerate parametric down-conversion to the optical mode at ω_a and the microwave mode (1).

This approximation allows us to assume that high-order terms are not resonantly coupled to the cavity, so the full Hamiltonian becomes

$$H = \hbar\omega_a a^\dagger a + \hbar(\omega_a - \Delta\omega)a_1^\dagger a_1 + \hbar(\omega_a + \Delta\omega)a_2^\dagger a_2 + \hbar\omega_b b^\dagger b - \hbar g(b + b^\dagger)(a + a_1 + a_2)^\dagger(a + a_1 + a_2)$$

(5)

5   Calculations and Results

5.1 $\frac{R(0)}{\eta}$ as a function of G_0

5.1.1   Deriving $\frac{R(0)}{\eta}$

Consider

$$\frac{d\alpha_-}{dt} = (-i\omega_0 - \gamma_0/2 - \gamma_a/2)\alpha_- - \sqrt{\gamma_a}A_{in}, \tag{6}$$

which is the dynamic equation for the cavity field amplitude as time progresses. This equation also takes into account the input from the fiber, which is coupled to the cavity. Here, A_{in} is the magnitude of the field input from the fiber, γ_a is the loss due to the coupling to the fiber, γ_0 is the total loss in the cavity, and ω is the cavity resonant frequency.

Next, if we Fourier transform equation 6, the left-hand side of the equation is represented in the frequency domain as follows:

$$- i\omega\alpha_- = (-i\omega_0 - \gamma_0/2 - \gamma_a/2)\alpha_- - \sqrt{\gamma_a}A_{in}, \tag{7}$$

where ω_0 is the cavity resonant frequency and ω is the frequency of the input field.

Then, the solution to the steady state equation (equation 6) is given by

$$\alpha_- = \frac{\sqrt{\gamma_a}A_{in}}{\left(i(\omega - \omega_0) - \frac{\gamma_a + \gamma_0}{2}\right)} \tag{8}$$

In order to find the number of photons, we need to take the absolute value squared of α_- and divide by the energy of the photon of interest. This leads to equation 45 from (1), which is given by

$$|\alpha_-^2| = \frac{\gamma_a p_{in}}{\hbar\omega_a\left(\delta^2 + \frac{\Gamma_a^2}{4}\right)} \tag{9}$$

Note that the γ_a in the denominator in equation 45 was replaced by Γ_a, which accounts for the total loss inside the cavity. Also, $\delta^2 = (\omega_{pump} - \omega_{cavity})^2$, which can range from 0 to $\frac{\Gamma_a}{2}$. Note that $\Gamma_a = \gamma_a + \gamma_0$.

Here, we assume zero detuning, and hence the cavity cooperativity parameter is given by

$$G_0 = \frac{4|g\alpha|^2}{\Gamma_a\Gamma_b}, \tag{10}$$

where g is the electro-optic coupling coefficient, $|\alpha|^2$ is the number of photons in the cavity, Γ_a is the total decay rates of the microwave mode, and Γ_b is the total decay rates of the optical mode.

Furthermore, at zero detuning, the electro-optic conversion efficiency is given by

$$R(0) = \frac{4\eta G_0}{(1 + G_0)^2},$$ (11)

where η is the intrinsic efficiency of the system and it is given by

$$\eta = \frac{\gamma_a \gamma_b}{\Gamma_a \Gamma_b}$$ (12)

5.1.2 Plotting G_0 vs. $\frac{R(0)}{\eta}$

One possibility to explore is how the plot of G_0 vs. $\frac{4G_0}{(1+G_0)^2}$ behaves when $\Gamma_a = \Gamma_b$. When $\Gamma_a = \Gamma_b = 10^8$ Hz, then we have the following plot
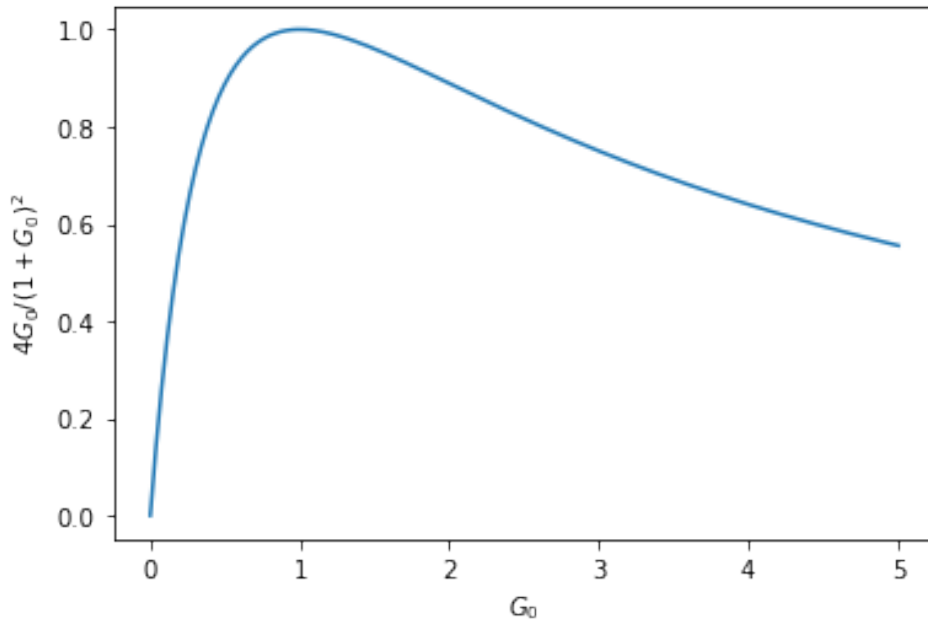

Figure 4: Plot of G_0 vs. $\frac{R(0)}{\eta}$ with $\Gamma_a = \Gamma_b$.

In this plot, the maximum value of $\frac{R(0)}{\eta}$ is 1, and it happens at $G_0 = 1$. This implies that

11

achieving cavity cooperativity value of 1 maximizes the electro-optic conversion efficiency.

5.2 $R(\omega)$ as a function of $\ln(\frac{\Gamma_b}{\Gamma_a})$ and Ω

5.2.1 Deriving $R(\omega)$ as a function of $\ln(\frac{\Gamma_b}{\Gamma_a})$ and Ω

In this plot, the x-axis is $\ln(\frac{\Gamma_b}{\Gamma_a})$. The y-axis is the normalized detuning frequency, which is given by

$$\Omega = \frac{2\omega}{\sqrt{\Gamma_a \Gamma_b}} \tag{13}$$

The third axis represents the electro-optic conversion efficiency, which is given by

$$R(\omega) = \frac{|g\alpha|^2 \gamma_a \gamma_b}{|(-i\omega - p_+)(-i\omega - p_-)|^2}, \tag{14}$$

where

$$P_\pm = -\frac{\Gamma_a + \Gamma_b}{4} \pm \sqrt{(\frac{\Gamma_a - \Gamma_b}{4})^2 - |g\alpha|^2} \tag{15}$$

are the poles of the transfer function.

Plug equation 15 into equation 14 to get

$$R(\omega) = \frac{|g\alpha|^2 \gamma_a \gamma_b}{|(-i\omega - (-\frac{\Gamma_a + \Gamma_b}{4} + \sqrt{(\frac{\Gamma_a - \Gamma_b}{4})^2 - |g\alpha|^2}))(-i\omega - (-\frac{\Gamma_a + \Gamma_b}{4} - \sqrt{(\frac{\Gamma_a - \Gamma_b}{4})^2 - |g\alpha|^2}))|^2}$$

$$R(\omega) = \frac{|g\alpha|^2 \gamma_a \gamma_b}{|(-i\omega + \frac{\Gamma_a + \Gamma_b}{4} - \sqrt{(\frac{\Gamma_a - \Gamma_b}{4})^2 - |g\alpha|^2})(-i\omega + \frac{\Gamma_a + \Gamma_b}{4} + \sqrt{(\frac{\Gamma_a - \Gamma_b}{4})^2 - |g\alpha|^2})|^2}$$

Let $A = -i\omega + \frac{\Gamma_a + \Gamma_b}{4}$, so we have

$$R(\omega) = \frac{|g\alpha|^2 \gamma_a \gamma_b}{|(A - \sqrt{(\frac{\Gamma_a - \Gamma_b}{4})^2 - |g\alpha|^2})(A + \sqrt{(\frac{\Gamma_a - \Gamma_b}{4})^2 - |g\alpha|^2})|^2}$$

$$R(\omega) = \frac{|g\alpha|^2 \gamma_a \gamma_b}{|A^2 - (\frac{\Gamma_a - \Gamma_b}{4})^2 + |g\alpha|^2|^2}$$

$$R(\omega) = \frac{|g\alpha|^2 \gamma_a \gamma_b}{|(-i\omega + \frac{\Gamma_a + \Gamma_b}{4})^2 - (\frac{\Gamma_a - \Gamma_b}{4})^2 + |g\alpha|^2|^2}$$

$$R(\omega) = \frac{|g\alpha|^2 \gamma_a \gamma_b}{|-\omega^2 - \frac{i\omega\Gamma_a}{2} + \frac{\Gamma_a^2}{16} - \frac{i\omega\Gamma_b}{2} + \frac{\Gamma_a\Gamma_b}{8} + \frac{\Gamma_b^2}{16} - \frac{\Gamma_a^2}{16} + \frac{\Gamma_a\Gamma_b}{8} - \frac{\Gamma_b^2}{16} + |g\alpha|^2|^2}$$

$$R(\omega) = \frac{|g\alpha|^2 \gamma_a \gamma_b}{|-\omega^2 - \frac{i\omega\Gamma_a}{2} - \frac{i\omega\Gamma_b}{2} + \frac{\Gamma_a\Gamma_b}{4} + |g\alpha|^2|^2}$$

$$R(\omega) = \frac{|g\alpha|^2 \gamma_a \gamma_b}{|-i(\frac{\omega}{2}(\Gamma_a + \Gamma_b)) + \frac{\Gamma_a\Gamma_b}{4} - \omega^2 + |g\alpha|^2|^2}$$

Let $B = \frac{\Gamma_a\Gamma_b}{4} - \omega^2 + |g\alpha|^2$ and $C = \frac{\omega}{2}(\Gamma_a + \Gamma_b)$ then we have

$$R(\omega) = \frac{|g\alpha|^2 \gamma_a \gamma_b}{|-iC+B|^2}$$

$$R(\omega) = \frac{|g\alpha|^2 \gamma_a \gamma_b}{C^2 + B^2}$$

Plug the values of B and C back again to get

$$R(\omega) = \frac{|g\alpha|^2 \gamma_a \gamma_b}{(\frac{\omega}{2}(\Gamma_a + \Gamma_b))^2 + (\frac{\Gamma_a \Gamma_b}{4} - \omega^2 + g^2\alpha^2)^2} \tag{16}$$

The goal here is to write $R(\omega)$ as a function of $\ln(\frac{\Gamma_b}{\Gamma_a})$ and Ω. To that end, divide equation 16 by $\frac{1}{\Gamma_a^2}$ to get

$$R(\omega)\Gamma_a^2 = \frac{|g\alpha|^2 \gamma_a \gamma_b}{\frac{1}{\Gamma_a^2}\left((\frac{\omega}{2}(\Gamma_a + \Gamma_b))^2 + (\frac{\Gamma_a \Gamma_b}{4} - \omega^2 + g^2\alpha^2)^2\right)}$$

$$R(\omega)\Gamma_a^2 = \frac{|g\alpha|^2 \gamma_a \gamma_b}{(\frac{\omega}{2}\frac{(\Gamma_a + \Gamma_b)}{\Gamma_a})^2 + (\frac{\Gamma_a \Gamma_b}{4\Gamma_a} - \frac{\omega^2}{\Gamma_a} + \frac{g^2\alpha^2}{\Gamma_a})^2}$$

$$R(\omega)\Gamma_a^2 = \frac{|g\alpha|^2 \gamma_a \gamma_b}{(\frac{\omega}{2}(1 + \frac{\Gamma_b}{\Gamma_a}))^2 + (\frac{\Gamma_b}{4\Gamma_a} - \frac{\omega^2}{\Gamma_a} + \frac{g^2\alpha^2}{\Gamma_a})^2},$$

where $\Gamma_a = \sqrt{\frac{\Gamma_a \Gamma_b}{\frac{\Gamma_b}{\Gamma_a}}}$, so we get

$$R(\omega) = \frac{|g\alpha|^2 \gamma_a \gamma_b}{\Gamma_a^2 \left(\frac{\omega}{2}(1 + \frac{\Gamma_b}{\Gamma_a}) \right)^2 + \left(\frac{\Gamma_b}{4\Gamma_a} - \frac{\omega^2}{\Gamma_a} + \frac{g^2\alpha^2}{\Gamma_a} \right)^2 \right)}$$

$$R(\omega) = \frac{|g\alpha|^2 \gamma_a \gamma_b}{\left(\left(\frac{\omega}{2}(1 + \frac{\Gamma_b}{\Gamma_a}) \right)^2 + \left(\frac{\Gamma_b}{4\Gamma_a} - \frac{\omega^2}{\Gamma_a} + \frac{g^2\alpha^2}{\Gamma_a} \right)^2 \right) \times \left(\frac{\Gamma_a \Gamma_b}{\frac{\Gamma_b}{\Gamma_a}} \right)}$$

5.2.2 Plotting $R(\omega)$ as a function of $\ln(\frac{\Gamma_b}{\Gamma_a})$ and Ω
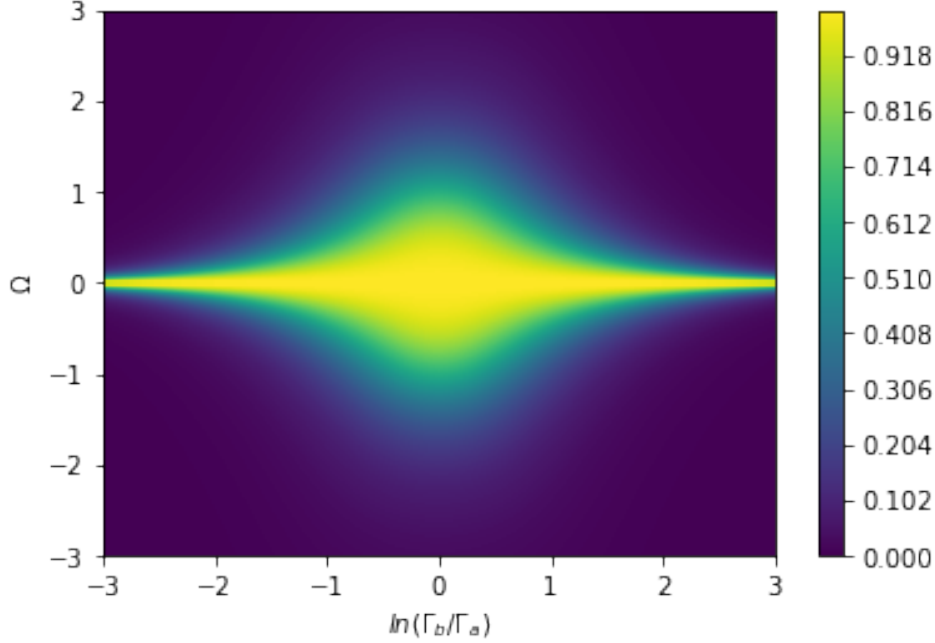

Figure 5: Plot of $R(\omega)$ as a function of $\ln(\frac{\Gamma_b}{\Gamma_a})$ vs. Ω.

In this plot, the maximum electro-optic conversion efficiency of 1 is reached when $\Gamma_a = \Gamma_b$ at zero detuning frequency. This result agrees with Figure 3, where the maximum conversion efficiency is achieved when $\Gamma_a = \Gamma_b$. As the difference between Γ_a and Γ_b increases, the efficiency is equal to 1 as long as $\Omega = 0$. However, as Ω increase or decreases, the conversion efficiency drastically drops. Therefore, this plot suggests that achieving a value of $\Omega = 0$ is the most important component to maximize conversion efficiency.

5.2.3 Conversion Efficiency when $(\frac{\Gamma_a - \Gamma_b}{4})^2 \gg |g\alpha|^2$

In the case where $(\frac{\Gamma_a - \Gamma_b}{4})^2 \gg |g\alpha|^2$, we get the following plot:
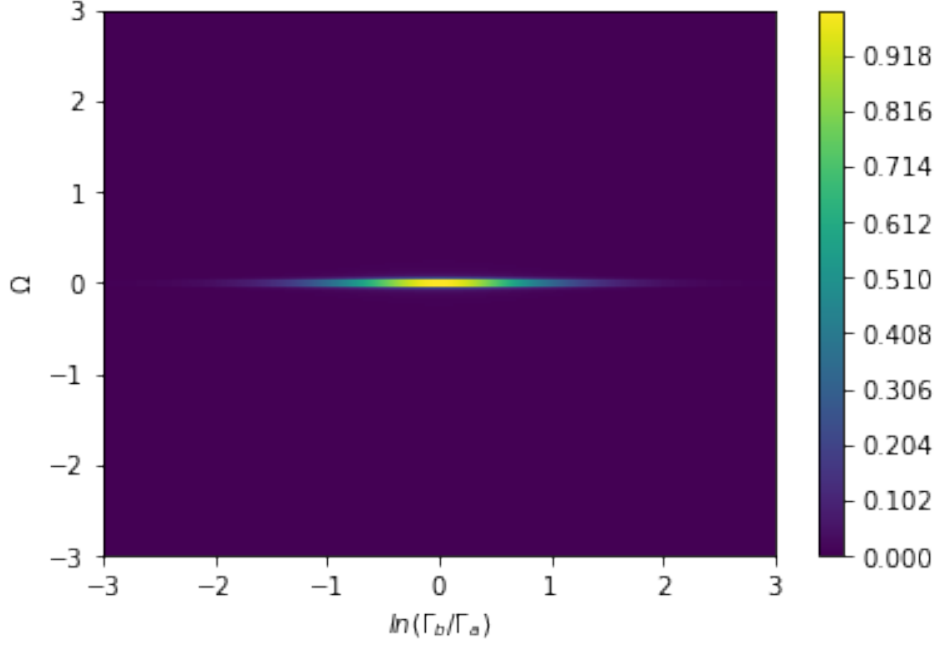
Figure 6: Plot of the case when $(\frac{\Gamma_a - \Gamma_b}{4})^2 \gg |g\alpha|^2$.

In this plot, $g = 100$, $\gamma_a = 10^7$ Hz, $\gamma'_a = 10^7$ Hz, $\gamma_b = 10^6$ Hz, $\gamma'_b = 10^7$ Hz, so $\left(\frac{\Gamma_a - \Gamma_b}{4}\right)^2 \backsim 10^{13}$ Hz. Additionally, $\alpha^2 = 10^4$, so $|g\alpha|^2 \backsim 10^{12}$. We see in this case that the conversion efficiency is considerably low compared to previous plots. However, the highest conversion efficiency was achieved when $\ln\left(\frac{\Gamma_b}{\Gamma_a}\right) = 0$, meaning that $\Gamma_a = \Gamma_b$.

5.2.4 Conversion Efficiency when $|g\alpha|^2 \gg (\frac{\Gamma_a - \Gamma_b}{4})^2$

In the case where $|g\alpha|^2 \gg (\frac{\Gamma_a - \Gamma_b}{4})^2$, we get the following plot:
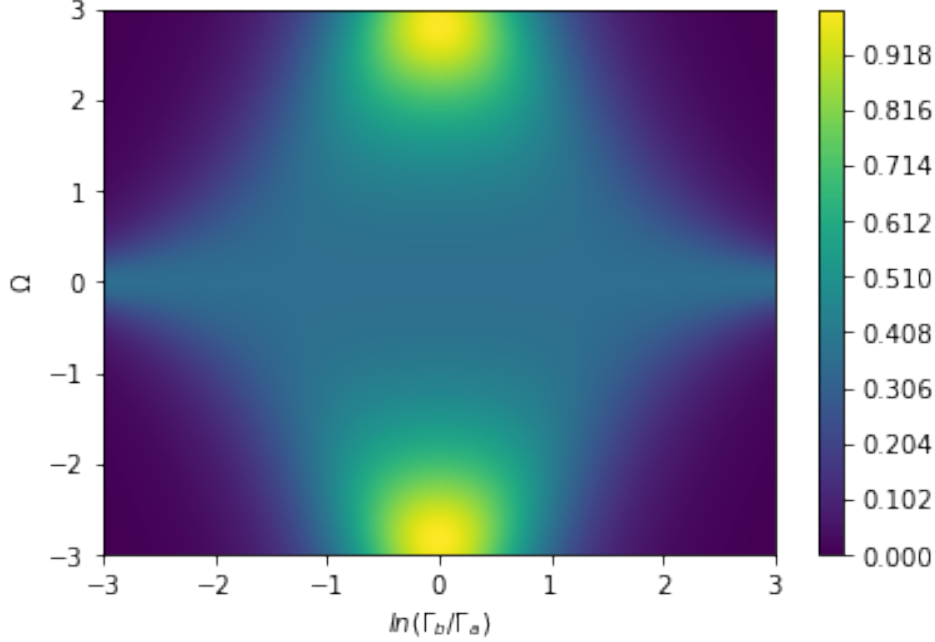

Figure 7: Plot of the case when $|g\alpha|^2 \gg (\frac{\Gamma_a - \Gamma_b}{4})^2$.

In this plot, $g = 100$, $\gamma_a = 10^7$ Hz, $\gamma_a' = 10^7$ Hz, $\gamma_b = 10^6$ Hz, $\gamma_b' = 10^7$ Hz, so $\left(\frac{\Gamma_a - \Gamma_b}{4}\right)^2 \backsim$ 10^{13} Hz. Additionally, $\alpha^2 = 10^{10}$, so $|g\alpha|^2 \backsim 10^{24}$. We see in this case that the conversion efficiency is no longer maximized when $\Omega = 0$ (as is the case in Figure 6) because of the splitting of the poles. Furthermore, the highest conversion efficiency values, which are still quite low, happen everywhere regardless of the value of $\ln\left(\frac{\Gamma_b}{\Gamma_a}\right)$.

5.2.5   Pole Splitting

It seems like the number of photons in the cavity is one of the factors that determine whether the poles will split. This behavior of pole splitting happens when $|\alpha|^2$ is about $10^{9.15}$.
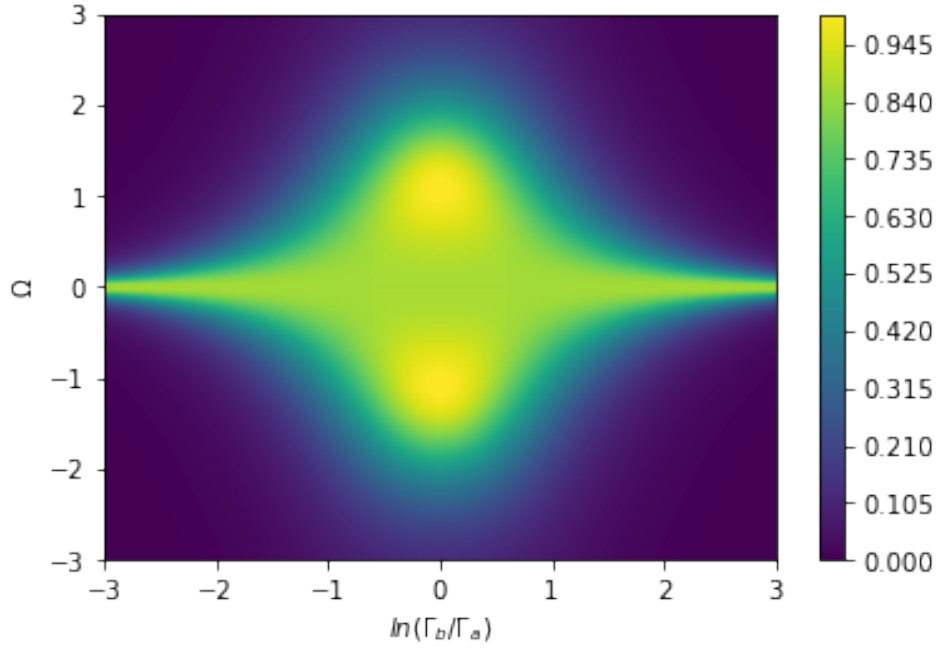

Figure 8: Splitting of Poles when the number of photons inside the cavity is $5 \times 10^{9.5}$ and $g = 100$.

Another factor determining is g. When $|\alpha|^2 = 10^9$ and $g = 100$, there is no pole splitting. However, if we keep $|\alpha|^2$ at 10^9 and make $g = 120$, then we observe the poles splitting. The following plot shows the behavior when $g = 170$
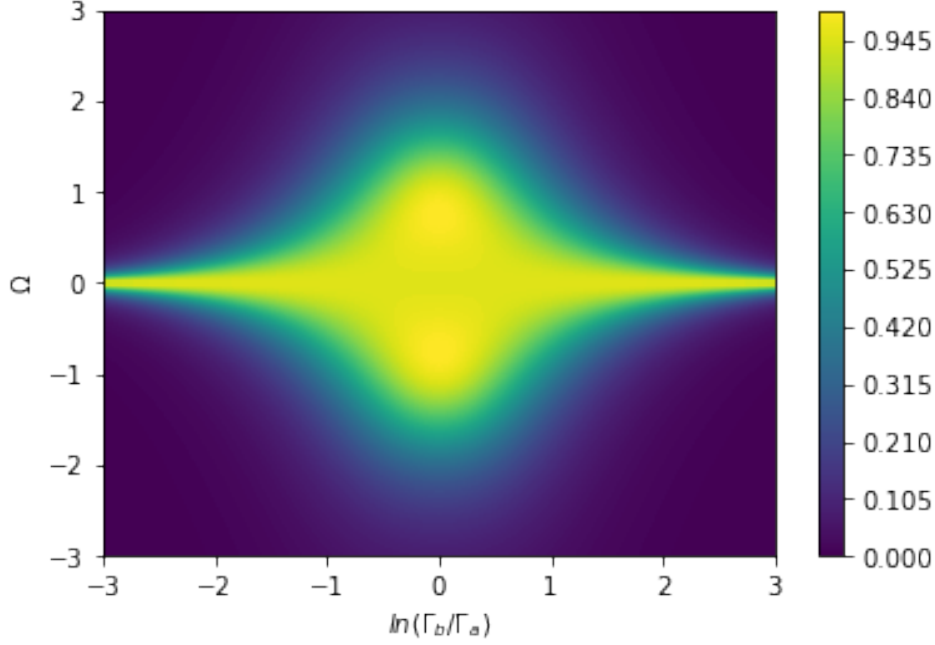
Figure 9: Splitting of Poles when the number of photons inside the cavity is 5×10^9 and $g = 170$.

5.2.6 Data Normalization:

In producing the third axis $R(\omega)$ of Figures $6 - 10$, the data was normalized using the following function:

$$\frac{d - d_{min}}{d_{max} - d_{min}}$$

, where d is a given data point, d_{min} is the minimum value of $R(\omega)$, and d_{max} is the maximum value of $R(\omega)$. This function was used because the maximum electro-optic conversion efficiency $R(\omega)$ was greater than 1 at times, which is physically unrealistic because it defies the energy conservation principle. The function preserves the behavior of the plots and ensures that the highest value of $R(\omega)$ does not exceed 1.

6 Conclusion

Our work utilizes a full quantum treatment of the electro-optic effect, which helped us study the parameter regime of decay rates. Specifically, we considered how these parameter regimes relate to figures of merit that indicate the cavity geometry (i.e., electro-optic conversion efficiency and cavity cooperativity). Finding the optimal values of these figures of merit is useful in improving the transduction behavior of the cavity. From this work, there are a few conclusions to be made. First, maximum conversion efficiency happens at $G_0 = 1$. Since G_0 depends on the cavity geometry, then knowing the optimal value of G_0 could inform some aspects of the cavity design. Second, the poles of the transfer function of the cavity split when $|g\alpha^2| \gg (\frac{\Gamma_a - \Gamma_b}{4})^2$. This is useful because when the poles split, the maximum conversion efficiency does not happen when detuning (Ω) is zero. Finally, we found that the maximum conversion efficiency happens when $\Gamma_a = \Gamma_b$. Currently, in the lab, the limitation is in Γ_b because it is lower than Γ_a. Since we have seen that the maximum conversion efficiency happens when $\Gamma_a = \Gamma_b$, we need to bridge the gap between the two gammas.

7 Acknowledgments

References

[1] Tsang, Mankei. "Cavity Quantum Electro-Optics." *Physical Review A*, vol. 81, no. 6, 2010, https://doi.org/10.1103/physreva.81.063837.

[2] Tsang, Mankei. "Cavity Quantum Electro-Optics. II. Input-Output Relations between Traveling Optical and Microwave Fields." *Physical Review A*, vol. 84, no. 4, 2011, https://doi.org/10.1103/physreva.84.043845.

[3] Lauk, Nikolai, et al. "Perspectives on Quantum Transduction." *Quantum Science and Technology*, vol. 5, no. 2, 2020, p. 020501., https://doi.org/10.1088/2058-9565/ab788a.

[4] Mirhosseini, Mohammad, et al. "Quantum transduction of optical photons from a superconducting qubit", https://arxiv.org/pdf/2004.04838.pdf

[5] Shor, Peter W. "Polynomial-Time Algorithms for Prime Factorization and Discrete Logarithms on a Quantum Computer." *SIAM Review*, vol. 41, no. 2, 1999, pp. 303–332., https://doi.org/10.1137/s0036144598347011.

[6] Möller, Matthias, and Cornelis Vuik. "On the Impact of Quantum Computing Technology on Future Developments in High-Performance Scientific Computing." *Ethics and Information Technology*, vol. 19, no. 4, 2017, pp. 253–269., https://doi.org/10.1007/s10676-017-9438-0.

[7] Leontica, S., et al. "Simulating Molecules on a Cloud-Based 5-Qubit IBM-Q Universal Quantum Computer." *Communications Physics*, vol. 4, no. 1, 2021, https://doi.org/10.1038/s42005-021-00616-1.

[8] Leontica, S., et al. "Simulating Molecules on a Cloud-Based 5-Qubit IBM-Q

Universal Quantum Computer." *Communications Physics*, vol. 4, no. 1, 2021, https://doi.org/10.1038/s42005-021-00616-1.

[9] Bertaina, S., et al. "Rare-Earth Solid-State Qubits." *Nature Nanotechnology*, vol. 2, no. 1, 2007, pp. 39–42., https://doi.org/10.1038/nnano.2006.174.

[10] Kok, Pieter, et al. "Linear Optical Quantum Computing with Photonic Qubits." *Reviews of Modern Physics*, vol. 79, no. 1, 2007, pp. 135–174., https://doi.org/10.1103/revmodphys.79.135.

[11] Burnett, Jonathan J., et al. "Decoherence Benchmarking of Superconducting Qubits." *Npj Quantum Information*, vol. 5, no. 1, 2019, https://doi.org/10.1038/s41534-019-0168-5.

[12] Walmsley, Ian. "Photonic Quantum Technologies." *Photonics for Quantum*, 2021, https://doi.org/10.1117/12.2603525.

[13] Zorzetti, S., Wang, C., Gonin, I., Grassellino, A., Kazakov, S., Romanenko, A., amp; Yakovlev, V. (2022). High-efficiency microwave-optical quantum transduction based on a cavity electro-optic superconducting system with long coherence time. https://doi.org/10.21203/rs.3.rs-1810251/v1

[14] Romanenko, A., Pilipenko, R., Zorzetti, S., Frolov, D., Awida, M., Belomestnykh, S., Posen, S., amp; Grassellino, A. (2020). Three-dimensional superconducting resonators at $T < 20$ mK with Photon Lifetimes up to $\tau = 2$ s. http://dx.doi.org/10.1103/PhysRevApplied.13.034032